FEBRUARY 01 1972

Numerical Study of Sound Refraction by a Jet Flow. II. Wave Acoustics

L. K. Schubert

J. Acoust. Soc. Am. 51, 447–463 (1972)
https://doi.org/10.1121/1.1912862

Received 24 September 1971 7.10; 11.2; 11.7; 14.6

Numerical Study of Sound Refraction by a Jet Flow. II. Wave Acoustics

L. K. SCHUBERT*

University of Toronto, Institute for Aerospace Studies, Toronto, Canada

The equations appropriate to the propagation of sound in a realistic jet flow have been solved by finite-difference methods for the case of a sinusoidal point source on the axis of a subsonic jet. Each numerical solution provides detailed phase and amplitude information throughout the sound field. At the high-frequency limit the finite-difference results agree with ray-tracing results. Also, the computed farfield directivity patterns generally agree with available experimental data and lend further support to the view that the downstream "valley" in jet noise is due to refraction rather than to the inherent directivity of the sound generated within the region of turbulence. Unexpected findings are that the flow beyond 100 nozzle diameters continues to deepen the refraction valley significantly, and that the sound-pressure level reduction at a fixed point on the axis at first increases as the source is moved downstream from the nozzle. For the application of the refraction results to the computation of jet noise directivity, it is found that the distortion of the constant phase surfaces can be neglected except at high frequencies.

INTRODUCTION

The motivation for the present study of acoustic radiation from a simple source in a jet flow has been stated in a companion paper treating the high-frequency limit.[1] Briefly, the objective is to complement and extend experimental results[2–6] and thereby to corroborate the refraction interpretation[7–10] of the downstream "valley" in jet noise.

As in most of the cited experiments, the model consists of a harmonic point source located on the axis of an axisymmetric jet flow.[11] A distinctive feature of the present study is the use of entirely realistic velocity and temperature profiles. Earlier studes[12–16] were based on highly idealized flow models (e.g., a nonspreading jet) and exaggerated the refraction effects by orders of magnitude. The physical model in principle admits turbulence, but turbulent scattering effects are suppressed in the final wave equation. To avoid the boundary condition of a solid jet nozzle, an unconfined convergent flow which supplies the jet flow is presumed to lie upstream of the nozzle plane. The exact nature of this "antijet" has been found to be unimportant as far as the downstream sound field is concerned. A constant-momentum antijet and a constant mass-flow antijet gave virtually indistinguishable results.

At the high-frequency limit the pressure field of the source can be computed by ray-tracing methods. Such geometric-acoustics solutions are available from Ref. 1; they should be in agreement with frequency-dependent results in the high-frequency limit. However, the frequencies of interest in jet noise are for the most part much too low for the application of ray-acoustics methods; instead a full wave-acoustics approach is required.

To simplify this task it is advantageous to combine the basic fluid-dynamical equations into a single wave equation involving a single dependent variable. Two such wave equations are considered here, one expressed in terms of acoustic pressure and the other in terms of Obukhov's quasi velocity potential.[17] Both versions are approximate; in fact, no exact wave equation exists for a flow with vorticity. The quasipotential formulation, although based on more restrictive physical assumptions, is computationally more convenient than the pressure formulation; therefore little use was made of the pressure formulation, except as a check on the quasipotential formulation where the latter is theoretically suspect.

In view of the complexity of the functions describing the flow field, a solution by numerical finite-difference methods was sought. The two versions of the wave equation were treated identically. First the time dependence $e^{-i\omega t}$ was divided out. There resulted a complex elliptic partial differential equation in the complex amplitude B of the pressure or quasipotential. Quantities related

to the phase and amplitude of B were chosen as new dependent variables. Unlike the sinuous variable B, these quantities are spatially monotonic over regions large compared with the wavelength. Even though the transformed wave equation is nonlinear, this fact facilitated the application of finite-difference methods by greatly reducing the required number of grid points. The difference equations approximating the differential equation (numbering 578 in most cases) were solved by nonlinear block relaxation using a Newton-like method.

I. DERIVATION, TRANSFORMATION, AND DISCRETIZATION OF CONVECTED WAVE EQUATION

A. Pressure Formulation and Obukhov's Quasipotential

The convected wave equation for uniform flow,[17]

$$\frac{1}{\bar{a}^2}\left(\frac{\partial^2 p^{(1)}}{\partial t^2}+2U\frac{\partial^2 p^{(1)}}{\partial x_1 \partial t}+U^2\frac{\partial^2 p^{(1)}}{\partial x_1^2}\right)-\nabla^2 p^{(1)}=0 \quad (1)$$

expressed in terms of pressure as above or in terms of an acoustic velocity potential Π, has sometimes been successfully applied to shear-flow problems.[18] This is somewhat surprising, since no velocity potential exists in a vortical flow. Nevertheless, Eq. 1 apparently accounts for most of the refraction and diffraction due to spatial variations of U and $\bar{a}^2$ in a jet flow. This conclusion has been reached after a careful numerical study of more accurate versions of the convected wave equation, which are derived below.

The effects of turbulent scattering will ultimately be suppressed by dropping products of turbulent quantities with acoustic perturbation quantities from the wave equation. This is not equivalent to the neglect of turbulent velocity fluctuations in the physical model. In fact, a time-averaged jet flow would violate the fluid-dynamical conservation equations.

Viscosity and heat conduction will be neglected herein. Their roles in the transport of momentum and energy within the jet flow are very minor compared to that of turbulent mixing. As far as the sound propagation is concerned, viscosity and heat conduction merely contribute (along with molecular relaxation effects) to the attenuation of sound at large distances.

The nonviscous momentum equation states that

$$\frac{Dv_i}{Dt}\equiv\frac{\partial v_i}{\partial t}+v_j\frac{\partial v_i}{\partial x_j}=-\frac{1}{\rho}\frac{\partial p}{\partial x_i}. \quad (2)$$

Differentiation with respect to x_i and substitution of the continuity equation in the form

$$\frac{\partial v_i}{\partial x_i}=-\frac{1}{\rho}\frac{D\rho}{Dt} \quad (3)$$

then gives

$$-\frac{D}{Dt}\left(\frac{1}{\rho}\frac{D\rho}{Dt}\right)+\frac{\partial v_j}{\partial x_i}\frac{\partial v_i}{\partial x_j}=\frac{1}{\rho^2}\frac{\partial \rho}{\partial x_i}\frac{\partial p}{\partial x_i}-\frac{1}{\rho}\frac{\partial^2 p}{\partial x_i \partial x_i}. \quad (4)$$

The neglect of viscosity and heat conduction leads to the simple energy equation[17]

$$Ds/Dt=0, \quad (5)$$

where s is the instantaneous local entropy. Consequently the equation of state, applied to a moving particle of fluid, becomes

$$\frac{D\rho}{Dt}=\frac{1}{a^2}\frac{Dp}{Dt}. \quad (6)$$

One can therefore expand the first term in Eq. 4 as

$$\frac{D}{Dt}\left(\frac{1}{\rho}\frac{D\rho}{Dt}\right)=\frac{1}{\rho a^2}\frac{D^2 p}{Dt^2}-\frac{1}{\rho^2 a^4}\left(\frac{Dp}{Dt}\right)^2+\frac{1}{\rho}\frac{Da^{-2}}{Dt}\frac{Dp}{Dt}$$
$$=\frac{1}{\rho a^2}\frac{D^2 p}{Dt^2}-\frac{\gamma}{\rho^2 a^4}\left(\frac{Dp}{Dt}\right)^2, \quad (7)$$

where the isentropic relation for an ideal gas $\delta a^{-2}=-(\gamma-1)/(\rho a^4)\delta p$ has been used.

The second term of the right-hand side of Eq. 7 can be neglected if it is supposed that fractional pressure changes in the jet are very small, i.e., $(p-p_0)/p_0=\epsilon f(\mathbf{x},t)$ where $\epsilon\ll 1$ and $f\sim 0(1)$. In that case $Dp/Dt\sim\epsilon p_0\omega f$, $D^2p/Dt^2\sim\epsilon p_0\omega^2 f$, and the ratio of the second term to the first $\sim(fp_0/p)\epsilon\ll 1$. This is rather a loose argument, since the symbol p lumps together aerodynamic and acoustic components. In a more careful treatment one finds that the quadratic term in Eq. 7 merely adds terms involving mean pressure gradients to the wave equation, and that all of these terms can be neglected under the somewhat more stringent assumption that fractional mean pressure variations are small compared to variations in the mean velocity ratio.[19]

Substituting Eq. 7, without the quadratic term, into Eq. 4 one obtains

$$\frac{1}{a^2}\frac{D^2 p}{Dt^2}-\frac{\partial^2 p}{\partial x_i \partial x_i}=\rho\frac{\partial v_i}{\partial x_j}\frac{\partial v_j}{\partial x_i}-\frac{1}{\rho}\frac{\partial \rho}{\partial x_i}\frac{\partial p}{\partial x_i}. \quad (8)$$

This of course is equivalent to Lighthill's equation[20] and its variants, although the demonstration of equivalence in the general case (nonuniform mean density) by expansion of the Lighthill source term $\partial^2(\rho v_i v_j)/\partial x_i \partial x_j$ and conversion from density to pressure on the left-hand side is more difficult than the derivation of either equation. Phillips' variant of the wave equation,[21] however, closely resembles the present version. Note that the right-hand side of Eq. 8 includes not only sound *generating* terms, but also sound *propagating* terms, such

as $\bar{\rho}(\partial U/\partial x_2)(\partial u_2/\partial x_1)$ (where U and u_2 are mean and acoustic velocity components).

When D/Dt is expanded, Eq. 8 becomes

$$\frac{1}{a^2}\left(\frac{\partial^2 p}{\partial t^2}+2v_i\frac{\partial^2 p}{\partial x_i \partial t}+v_i v_j\frac{\partial^2 p}{\partial x_i \partial x_j}\right)-\frac{\partial^2 p}{\partial x_i \partial x_i} = \rho\frac{\partial v_i}{\partial x_j}\frac{\partial v_j}{\partial x_i}-\frac{1}{\rho}\frac{\partial \rho}{\partial x_i}\frac{\partial p}{\partial x_i}. \quad (9)$$

The term $(Dv_i/Dt)(\partial p/\partial x_i)$ resulting from the second application of the D/Dt operator has been discarded, since it is equal to $-\rho^{-1}(\partial p/\partial x_i)^2$ by Eq. 2. Its retention would lead to further terms in the final wave equation involving mean pressure gradients. Like those resulting from the retention of the last term in Eq. 7, they turn out to be negligible.

One may replace p, v_i and ρ by $p^{(0)}+p^{(1)}$, w_i+u_i and $\rho^{(0)}+\rho^{(1)}$, respectively. The first part of each sum corresponds to the value in the absence of *injected* sound; the second part is the additional perturbation due to the injected sound. Neglecting second-order terms and products of acoustic perturbations with pressure gradients, and subtracting the equation valid when no injected sound is present (this automatically eliminates terms associated with the generation, propagation, and scattering of aerodynamic jet noise), one obtains

$$\frac{1}{a^2}\left(\frac{\partial^2 p^{(1)}}{\partial t^2}+2w_i\frac{\partial^2 p^{(1)}}{\partial x_i \partial t}+w_i w_j\frac{\partial^2 p^{(1)}}{\partial x_i \partial x_j}\right)-\frac{\partial^2 p^{(1)}}{\partial x_i \partial x_i} = \rho^{(1)}\frac{\partial w_i}{\partial x_j}\frac{\partial w_j}{\partial x_i}+2\rho^{(0)}\frac{\partial w_i}{\partial x_j}\frac{\partial u_j}{\partial x_i}-\frac{1}{\rho^{(0)}}\frac{\partial \rho^{(0)}}{\partial x_i}\frac{\partial p^{(1)}}{\partial x_i}. \quad (10)$$

Scattering of the injected sound by the turbulence can now be suppressed by replacing a^2, $\rho^{(0)}$, and w_i by their local time averages $\bar{a}^2$, $\bar{\rho}$, and U_i. If in addition $U_i \approx U\delta_{i1}$ (i.e., unidirectional flow), then Eq. 10 becomes

$$\frac{1}{\bar{a}^2}\left(\frac{\partial^2 p^{(1)}}{\partial t^2}+2U\frac{\partial^2 p^{(1)}}{\partial x_1 \partial t}+U^2\frac{\partial^2 p^{(1)}}{\partial x_1^2}\right)-\frac{\partial^2 p^{(1)}}{\partial x_i \partial x_i} = \rho^{(1)}\left(\frac{\partial U}{\partial x_1}\right)^2+2\bar{\rho}\frac{\partial U}{\partial x_j}\frac{\partial u_j}{\partial x_1}-\frac{1}{\bar{\rho}}\frac{\partial \bar{\rho}}{\partial x_i}\frac{\partial p^{(1)}}{\partial x_i}. \quad (11)$$

Since the flow in a jet is nearly parallel, $\partial U/\partial x_1$ is small [$|\partial(U/U_j)/\partial(x_1/D)|<0.1$ for the jet; by contrast $|\partial(U/U_j)/\partial(x_2/D)|_{\max}\approx 1.2$ at the end of the mixing region] so that it seems reasonable to retain only $2\bar{\rho}\partial U/\partial z\ \partial u_z/\partial x_1$, where $z=(x_2^2+x_3^2)^{\frac{1}{2}}$, of the second source term in Eq. 11. The first source term is appreciable only at very low frequencies, as may be ascertained by writing $\rho^{(1)}$ as $(\bar{a}^2)^{-1}p^{(1)}$ and comparing with the first term of the left-hand side (term is important for $\omega \leqslant \partial U/\partial x_1$, i.e., $f \leqslant 0.016 M_j a_j/D$; e.g., at $M_j=0.5$, $D=0.75$ in., the threshold is $f=142$ Hz).

Thus one arrives at the approximate wave equation

$$\frac{1}{\bar{a}^2}\left(\frac{\partial^2 p^{(1)}}{\partial t^2}+2U\frac{\partial^2 p^{(1)}}{\partial x_1 \partial t}+U^2\frac{\partial^2 p^{(1)}}{\partial x_1^2}\right)-\frac{\partial^2 p^{(1)}}{\partial x_i \partial x_i} = 2\bar{\rho}\frac{\partial U}{\partial z}\frac{\partial u_z}{\partial x_1}-\frac{1}{\bar{\rho}}\frac{\partial \bar{\rho}}{\partial x_i}\frac{\partial p^{(1)}}{\partial x_i}. \quad (12)$$

Because of the presence of the shear term

$$2\bar{\rho}\partial U/\partial z\ \partial u_z/\partial x_1,$$

this equation can be solved independently of the momentum equation only under conditions when (i) $\partial u_z/\partial x_1$ is expressible in terms of $p^{(1)}$ or (ii) the effect of the shear term on the solution is slight (this can occur even when the shear term is not small).

In general (i) is false. However, when the Mach number $M_j \lesssim \sim 0.1$ and the mean density is uniform, $\partial u_z/\partial x_1$ is approximately[22] $(i\omega\bar{\rho})^{-1}\partial^2 p^{(1)}/\partial x_1 \partial z$. The main use made of this approximation was to determine conditions under which (ii) holds and to check the quasipotential formulation discussed below. The inclusion of the approximation in the wave equation ultimately leads to a considerable complication of the numerical computations.

Regarding (ii), it turns out that both the shear term and the density gradient term on the right-hand side of Eq. 12 vary like ω^{-1} compared to terms on the left-hand side (note that they contain only singly differentiated perturbation quantities, whereas all terms on the left-hand side contain double derivatives). Consequently their relative contributions to the solution should diminish with increasing frequency. Studies of both terms by the finite-difference methods described herein are reported in Ref. 22. An integral estimate of shear term effects, which corroborates the finite-difference results, is also given there. The conclusions are that the density gradient term is unimportant at jet noise frequencies, whereas the shear term appreciably enhances the downstream radiation at the expense of upstream radiation. This reduces the depth of the axial valley by about 1.8 dB for each 0.1 increase in Mach number, irrespective of the frequency. For frequencies $f<0.5a/D$ ($\lambda>2D$) the reduction becomes too large a fraction of the over-all valley depth to be ignored. This frequency limit, though established for low Mach numbers only, is thought to be typical at higher Mach numbers as well, since both the shear term and the main refraction term in the wave equation are proportional to M_j.

The limited usefulness of the pressure formulation of Eq. 12 without the shear term, and the awkwardness of computations with the low Mach number approximation to the shear term, motivated an attempt to formulate the convected wave equation in terms of some quasi-velocity potential. It is shown in Ref. 22 that assumptions of uniform entropy, small w and w-derivatives ($|\mathbf{w}|\ll a$, $|\nabla\times\mathbf{w}|\ll\omega$, $|(\mathbf{w}\cdot\nabla)(\nabla\times\mathbf{w})|\ll\omega|\nabla\times\mathbf{w}|$), neg-

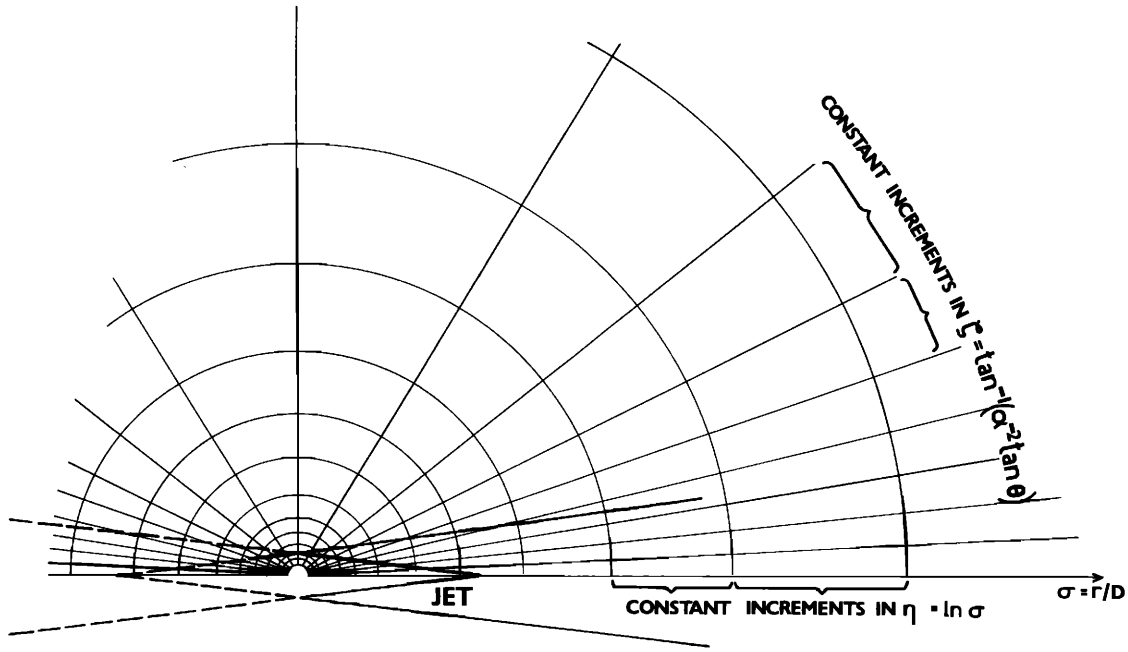

FIG. 1. The finite difference grid. Only the first 13 of the 19 circumferential grid lines are shown. Here the source is at the center of the nozzle.

ligible turbulent scattering, and unidirectional mean flow lead to the equation

$$\frac{1}{a^2}\left(\frac{\partial^2\Pi}{\partial t^2}+2U\frac{\partial^2\Pi}{\partial x_1\partial t}+U^2\frac{\partial^2\Pi}{\partial x_1^2}\right)$$

$$-\frac{\partial^2\Pi}{\partial x_i\partial x_i}-\frac{i}{\omega}\frac{\partial^2 U}{\partial x_i\partial x_i}\frac{\partial\Pi}{\partial x_1}=0 \quad (13)$$

for a quasipotential Π related to the acoustic pressure and velocity by

$$\frac{p^{(1)}}{p^{(0)}}=\frac{\partial\Pi}{\partial t}+w_i\frac{\partial\Pi}{\partial x_i} \quad (14)$$

and

$$u_i=-\frac{\partial\Pi}{\partial x_i}+u_i'$$

$$\approx-\frac{\partial\Pi}{\partial x_i}+\int^t\left(\frac{\partial w_i}{\partial x_i}\frac{\partial\Pi}{\partial x_j}-\frac{\partial w_j}{\partial x_i}\frac{\partial\Pi}{\partial x_j}\right)dt. \quad (15)$$

Π is a special case of Obukhov's quasipotential,[17] for nearly uniform density and a sinusoidal source of sound.

For constant density, Eq. 13 is identical in form to the pressure equation (Eq. 12) except for the extra term involving the Laplacian of the mean velocity. Here the extra term is of order ω^{-2} compared to other terms, so that its contribution to the solution should again diminish with increasing frequency. Numerical studies of this contribution (which are relatively easy in this case since only the single dependent variable Π is involved) have shown that it is qualitatively similar to the contribution of the shear term in the pressure formulation. However, it diminishes the depth of the axial valley by only about 1 dB for each 0.1 increase in the Mach number, so that it can be ignored down to lower frequencies ($f\sim 0.15a/D$, or $\lambda\sim 7D$). Judging from comparisons of computed results (obtained by the finite-difference methods to be described) with the experimental evidence,[2–6] it may be permissible to omit the extra term from Eq. 13 at even lower frequencies. Physically, this suggests that the part of the sound field induced by the mean flow vorticity is itself solenoidal. For if the divergence of u_i' in Eq. 15 is assumed to vanish, then Eq. 13, without the last term, is satisfied irrespective of the Mach number.

In spite of its theoretical limitations, the potential formulation has been found to be consistent with the pressure formulation in all cases where the pressure formulation is demonstrably valid.[22] This includes high Mach number and high temperature cases. After the initial compatibility studies, therefore, most computations were done with the less cumbersome potential formulation.

Both formulations remain suspect at low frequencies ($f<0.15a/D$), when the Mach number is not low ($M>0.1$). Results in this regime appear to agree with experiment, but clearly cannot be considered reliable.

B. Transformations and Finite-Difference Formulation

If the harmonic sound field generated by the simple source is written as $p^{(1)}$ (or Π) $=B\exp(-i\omega t)$, then the

time dependence can be eliminated from the convected wave equation, so that Eq. 1 (or Eq. 13, without the last term) becomes

$$\nabla^2 B - M^2 \frac{\partial^2 B}{\partial \xi_1^2} + 2iMW \frac{\partial B}{\partial \xi_1} + W^2 B = 0 \qquad (16)$$

in terms of the dimensionless quantities $\xi_i = x_i/D$, $M = U/a$, and $W = \omega D/a$ (these are functions of position in general). Note that the three parameters $M_j = U_j/a_j$, $W_0 = \omega D/a_0$, and $C = a_j/a_0$ fully determine the solution for a given source position. The real and imaginary parts of Eq. 16 give two linear elliptic equations involving the real and imaginary parts of B.

Of the known methods for the approximate treatment of partial differential equations, a numerical finite-difference approach was judged to be the most easily implemented. A spherical polar grid was chosen since B is expected to be a simple function of the radial distance r for large r. This simplified the farfield boundary conditions. The grid lies between two source-centered circles, one of very small and one of very large radius. Appropriate boundary conditions on these circles are formulated later.

It was soon realized that an extremely large number of grid points (10^4 to 10^7, depending on the frequency) would be required to resolve the fluctuations in the sinuous variable

$$B = A \exp(i\Phi) = A \cos\Phi + iA \sin\Phi. \qquad (17)$$

On the other hand the amplitude A and phase Φ should vary monotonically with distance; if A is written as χ/σ and Φ as $\sigma\Psi$, where $\sigma = r/D$, then χ and Ψ should be nearly constant and a much coarser grid will suffice to delineate them. This advantage easily offsets the disadvantages associated with the nonlinearization of Eq. 16, which is a consequence of the transformation from B to χ and Ψ.

For convenience χ was replaced by its decibel value $S = \beta \ln(\chi/\chi_0)$, where β and χ_0 are constants. Now the largest variations in S and Ψ are expected to occur near $\sigma = 0$ and near $\tan\theta = 0$ where θ is the angle with the jet axis, while at larger values of σ and $\tan\theta$ these variations should subside. Thus the grid spacing may be allowed to increase with σ and $\tan\theta$. The transformations $\eta = \ln\sigma$ and $\tan\theta = \alpha^2 \tan\zeta$, where $\alpha^2 < 1$,[23] give the desired variations of the grid spacing in real space when constant spacing is used in η, ζ-space. The grid is shown in Fig. 1.

The foregoing transformations can be summarized as

$$B = \chi_0 \exp\left(\frac{S}{\beta} - \eta + ie^{\eta}\Psi\right),$$
$$\eta = \ln(\xi_1^2 + \xi_2^2 + \xi_3^2)^{\frac{1}{2}}, \qquad (18)$$
$$\zeta = \tan^{-1}\left[\frac{(\xi_2^2 + \xi_3^2)^{\frac{1}{2}}}{\alpha^2 \xi_1}\right],$$

and these convert Eq. 16 to the mildly nonlinear form

$$\begin{aligned}
&\frac{R^2 - M^2Q^2}{R^2}\frac{\partial^2 S}{\partial \eta^2} + 2M^2PQ\frac{\partial^2 S}{\partial \eta \partial \zeta} + R^2(R^2 - M^2P^2)\frac{\partial^2 S}{\partial \zeta^2} - \frac{R^2 + M^2P^2 - 3M^2Q^2}{R^2}\frac{\partial S}{\partial \eta} \qquad \text{Real}\\
&+\left[2PQ(\alpha^2 - \alpha^{-2})(R^2 - M^2P^2) + \frac{Q}{P}(R^2 - 4M^2P^2)\right]\frac{\partial S}{\partial \zeta} + \frac{1}{\beta}\left[\left(\frac{\partial S}{\partial \eta}\right)^2 + R^4\left(\frac{\partial S}{\partial \zeta}\right)^2 - \left(\frac{MQ}{R}\frac{\partial S}{\partial \eta} - MQR\frac{\partial S}{\partial \zeta}\right)^2\right] \qquad \text{Part}\\
&+\beta\left(\frac{M^2P^2 - 2M^2Q^2}{R^2} - e^{2\eta}\left\{\left(\Psi + \frac{\partial \Psi}{\partial \eta}\right)^2 + R^4\left(\frac{\partial \Psi}{\partial \zeta}\right)^2 - \left[\frac{MQ}{R}\left(\Psi + \frac{\partial \Psi}{\partial \eta}\right) - MPR\frac{\partial \Psi}{\partial \zeta} - W\right]^2\right\}\right) = 0,\\
&\frac{R^2 - M^2Q^2}{R^2}\frac{\partial^2 \Psi}{\partial \eta^2} + 2M^2PQ\frac{\partial^2 \Psi}{\partial \eta \partial \zeta} + R^2(R^2 - M^2P^2)\frac{\partial^2 \Psi}{\partial \zeta^2} + \frac{R^2 - M^2P^2 + M^2Q^2}{R^2}\frac{\partial \Psi}{\partial \eta} \qquad \text{Imaginary}\\
&+\left[\frac{Q}{P}(R^2 - 2M^2P^2) + 2PQ(\alpha^2 - \alpha^{-2})(R^2 - M^2P^2)\right]\frac{\partial \Psi}{\partial \zeta} - \frac{M^2P^2 - 2M^2Q^2}{R^2}\Psi - 2W\frac{MQ}{R} \qquad \text{Part}\\
&+\frac{2}{\beta}\left\{\frac{\partial S}{\partial \eta}\left(\Psi + \frac{\partial \Psi}{\partial \eta}\right) + \frac{\partial S}{\partial \zeta}\frac{\partial \Psi}{\partial \zeta}R^4 - \left[\frac{MQ}{R}\left(\Psi + \frac{\partial \Psi}{\partial \eta}\right) - MPR\frac{\partial \Psi}{\partial \zeta} - W\right]\left(\frac{MQ}{R}\frac{\partial S}{\partial \eta} - MPR\frac{\partial S}{\partial \zeta}\right)\right\} = 0
\end{aligned} \qquad (19)$$

where $P = \alpha \sin\zeta$, $Q = \alpha^{-1}\cos\zeta$, $R = (P^2 + Q^2)^{\frac{1}{2}}$. Inserting the usual finite difference approximations

$$\begin{aligned}
&\frac{\partial S}{\partial \eta} \approx \frac{S_{10} - S_{-10}}{2H}, \quad \frac{\partial S}{\partial \zeta} \approx \frac{S_{01} - S_{0-1}}{2K}; \quad \frac{\partial^2 S}{\partial \eta^2} \approx \frac{S_{10} - 2S_{00} + S_{-10}}{H^2},\\
&\frac{\partial^2 S}{\partial \zeta^2} \approx \frac{S_{01} - 2S_{00} + S_{0-1}}{K^2}; \quad \frac{\partial^2 S}{\partial \eta \partial \zeta} \approx \frac{S_{11} - S_{1-1} - S_{-11} + S_{-1-1}}{4HK},
\end{aligned} \qquad (20)$$

and similarly for Ψ for uniform grid spacing H and K in η and ζ, respectively, one obtains the discrete analogs $f_{\mathrm{Re}}(i,j)=f_{\mathrm{Im}}(i,j)=0$ corresponding to Eq. 19; f_{Re} and f_{Im}, often called "point residuals," are defined for each internal grid point (i,j). Explicit expressions are given in Ref. 22; the required additions to f_{Re} and f_{Im}, if it is desired to include the extra term $-i\omega^{-1}\nabla^2 U\partial\Pi/\partial x_1$ in the Π formulation, can also be found there. That the discrete equations are in fact approximations to the analytic equations, with errors of order H^2, K^2, and HK, follows from Taylor's theorem if it is assumed that the partial derivatives of S and Ψ, up to the fourth, are bounded in the domain of solution.

To complete the formulation of the discrete problem it remains to state the boundary conditions. Because of the axisymmetry of the source-jet configuration it is natural to restrict θ to the interval $0, \pi$. Thus there are three boundary segments: the innermost and outermost circumferential grid lines and the symmetry axis.

The inner boundary condition is critical in that it effectively specifies the characteristics of the source. Two questions arise in the formulation of this condition: what is the nearfield of a point source in an unbounded uniform flow, and how is this nearfield modified, if at all, by the presence of the jet edge and other nonuniformities in a jet flow?

In a recent theoretical note on moving point sources, Graham and Graham[24] have pointed out that the notion of a "simple source" in a uniform flow is not uniquely defined (except at the high-frequency limit). For example, the field of such a source may be construed as a discrete-tone Green's function for the convected wave equation with either *pressure* or *potential* as dependent variable; but it is easily verified that the solutions of $a^{-2}D^2p^{(1)}/Dt^2-\nabla^2p^{(1)}=\delta(\mathbf{x}-\mathbf{y})\exp(-i\omega t)$ and $a^{-2}D^2\Pi/Dt^2-\nabla^2\Pi=\delta(\mathbf{x}-\mathbf{y})\exp(-i\omega t)$ are not equivalent. It is not certain which choice corresponds more closely to experimental "simple sources." However, directivity patterns corresponding to different choices of theoretical source type show little difference in refraction effects; instead, the differences take the form of a general downstream enhancement (at the expense of upstream radiation) of greater or lesser magnitude. For consistency with earlier theoretical work, the Green's function for the potential (see, e.g., Refs. 14, 17) has been taken as basic here.

The question of possible effects of flow nonuniformities may be dealt with as follows. Consider an integral iteration in which the nearfield of the source is sought by regarding

$$[(\overline{a_s^2})^{-1}(2U_s\partial^2\Pi/\partial x_1\partial t+U_s{}^2\partial^2\Pi/\partial x_1{}^2)-(\bar{a}^2)^{-1}(2U\partial^2\Pi/\partial x_1\partial t+U^2\partial^2\Pi/\partial x_1{}^2)],$$

where the subscript s denotes values at the source, as a forcing term in the convected wave equation. If the potential corresponding to uniform velocity U_s and sound speed a_s is used as "zeroth" approximation, subsequent iterations are found to add terms at most of order $\ln r$. Thus the uniform-flow part of the solution, which is of order r^{-1}, predominates close to the source. This has been verified[22] for Moretti and Slutsky's analytical velocity potential corresponding to a point source in a nonspreading jet.[14]

The appropriate velocity potential in a uniform flow is

$$\Pi=\frac{q\exp\left\{-i\omega\left[t+\dfrac{r}{a}\dfrac{M\cos\theta-(1-M^2\sin^2\theta)^{\frac{1}{2}}}{1-M^2}\right]\right\}}{4\pi r(1-M^2\sin^2\theta)^{\frac{1}{2}}} \tag{21}$$

where q is the amplitude of the total volume flow away from the source. The transformation to S, Ψ satisfies $\Pi=\chi_0\exp[S/\beta-\eta+i(e^{\eta}\Psi-\omega t)]$ so that the inner boundary conditions for Π are

$$S=C_1-(\beta/2)\ln(1-M^2\sin^2\theta),\qquad \Psi=W\frac{(1-M^2\sin^2\theta)^{\frac{1}{2}}-M\cos\theta}{1-M^2}. \tag{22}$$

Equivalent conditions for $p^{(1)}$ can be obtained from $p^{(1)}=\bar{\rho}D\Pi/Dt$.[22] In order that Conditions 22 be approximately valid on the inner boundary, the radius of that boundary must be chosen small enough. Experimentation with various radii has shown that the value $r/D=0.25$ is generally adequate.

The outer boundary conditions were based on the expansions (at fixed θ)

$$S=S_\infty+S_1/\sigma+S_2/\sigma^2+\cdots,\qquad \Psi=\Psi_\infty+\Psi_1/\sigma+\Psi_2/\sigma^2+\cdots. \tag{23}$$

In most computations[25] the outer radius was $\sigma=r/D=100$. At this distance, the first two terms in the expansions were found to suffice, in that no reflections from the boundary were discernible. On the other hand, pronounced standing waves were produced if the expansions were truncated after the first term. The discrete analogs of Eq. 23, up to orders σ^{-1}, are found to be

$$S_{m,j}=\frac{4S_{m-1,j}-(2-H)S_{m-2,j}}{2+H},\quad j=2,3,\cdots,n-1,\qquad \Psi_{m,j}=\frac{4\Psi_{m-1,j}-(2-H)\Psi_{m-2,j}}{2+H},\quad j=2,3,\cdots,n-1, \tag{24}$$

where m and n are the number of circumferential and radial grid lines, respectively. When H is small, $S_{m,j}$ and $\Psi_{m,j}$ approach the values corresponding to linear extrapolation, so that the discretization error is of order H^2.

The usual method of extracting symmetry boundary conditions from the basic difference equations themselves, by applying the equations at points on the boundary and using mirror-image values at missing grid

points, fails in the present case. The reason is that the difference equations are identities on the jet axis. Axial values of S and Ψ were therefore computed by quadratic interpolation through the two nearest points on the same circumferential grid line, with a zero slope condition imposed at the axis. Thus the symmetry boundary conditions are

$$S_{i,1}=\frac{4S_{i,2}-S_{i,3}}{3},\quad \Psi_{i,1}=\frac{4\Psi_{i,2}-\Psi_{i,3}}{3},$$
$$i=2,3,\cdots,m, \quad (25)$$

and similarly for $S_{i,n}$ and $\Psi_{i,n}$. The discretization error in these approximations is of order K^4, since only even terms are present in the Taylor expansions of S and Ψ about $\zeta=0$.

The discretization error in the complete set of finite-difference equations is thus quadradic in the grid spacing. However, in view of the state of the art in proving the convergence of discrete solutions to the solutions of corresponding continuous problems, it will be assumed rather than proved that the solution of the present discrete problem converges. The plausibility of this assumption was confirmed by solving the discrete equations for a succession of grid densities and observing that the solution appeared to approach an asymptotic limit at small H, K. In the simple case of uniform flow, the asymptotic limit satisfactorily approximates the analytical solution, Eq. 21. For a jet flow the asymptotic limit is consistent with the experimental evidence and, at the high-frequency limit, with ray acoustics (see Sec. III).

II. SOLUTION OF NONLINEAR DIFFERENCE EQUATIONS

The Jacobian J of the system of algebraic equations derived from the discrete analogs of Eq. 19 and the boundary conditions satisfies none of the conditions usually postulated to ensure the stability of point or block iterative methods of solution. It is not symmetric, nor diagonally dominant (the largest elements, by several orders of magnitude, are those associated with the Ψ-derivatives of f_{Re}), nor positive definite, nor probably amenable to a regular splitting ($J=P-Q$; $P^{-1}, Q\geqslant 0$) as it contains positive off-diagonal elements.[26] The same is individually true of each quadrant of J, and of many of the tridiagonal blocks that constitute each quadrant.

Nevertheless, nonlinear block iteration can be made to work, if each block is chosen to consist of the equations corresponding to at least three neighboring radial grid lines. No viable alternative to this method was found; for example, minimization methods invariably stagnate at spurious minima.

The block iteration may be described as follows. Let x represent the unknowns on l adjacent radial mesh lines (numbered j, $j+1$, $\cdots$, $j+l-1$), i.e.,

$$x=(S_{1,j},S_{2,j},\cdots,S_{m-2,j};\ S_{1,j+1},S_{2,j+1},\cdots,S_{m-2,j+1};\ \cdots;$$
$$S_{1,j+l-1},S_{2,j+l-1},\cdots,S_{m-2,j+l-1};\ \Psi_{1,j},\Psi_{2,j},\cdots,\Psi_{m-2,j};$$
$$\Psi_{1,j+1},\Psi_{2,j+1},\cdots,\Psi_{m-2,j+1};\ \cdots;$$
$$\Psi_{1,j+l-1},\Psi_{2,j+l-1},\cdots,\Psi_{m-2,j+l-1})^T.$$

Also let f be the vector comprised of the "point residuals" $f_{\mathrm{Re}}(i,j)$ and $f_{\mathrm{Im}}(i,j)$ at the internal points of these grid lines, i.e.,

$$f=[f_{\mathrm{Re}}(1,j),f_{\mathrm{Re}}(2,j),\cdots,f_{\mathrm{Re}}(m-2,j);\ f_{\mathrm{Re}}(1,j+1),$$
$$f_{\mathrm{Re}}(2,j+1),\cdots,f_{\mathrm{Re}}(m-2,j+1);\ \cdots;$$
$$f_{\mathrm{Re}}(1,j+l-1),f_{\mathrm{Re}}(2,j+l-1),\cdots,$$
$$f_{\mathrm{Re}}(m-2,j+l-1);\ f_{\mathrm{Im}}(1,j),f_{\mathrm{Im}}(2,j),\cdots,$$
$$f_{\mathrm{Im}}(m-2,j);\ f_{\mathrm{Im}}(1,j+1),f_{\mathrm{Im}}(2,j+1),\cdots,$$
$$f_{\mathrm{Im}}(m-2,j+1);\ \cdots;\ f_{\mathrm{Im}}(1,j+l-1),$$
$$f_{\mathrm{Im}}(2,j+l-1),\cdots,f_{\mathrm{Im}}(m-2,j+l-1)]^T.$$

An "inner" iteration suppresses all components of f for a particular j, while the "outer" block iteration repeatedly carries j through the values $j=2,3,\cdots,n-l$. The inner iteration is

$$x^{(p+1)}=x^{(p)}+t^{(p)}d^{(p)}, \quad (26)$$

with $d^{(p)}$ obtained by direct solution of

$$A^{(p)}d^{(p)}=-f^{(p)}, \quad (27)$$

where $A^{(p)}$ is an approximation to J^{-1} and $t^{(p)}$ is a scalar chosen so that $\|f^{(p+1)}\|\leqslant\|f^{(p)}\|$, thus ensuring nondivergence of the inner iteration. For $A^{(p)}\equiv[J^{(p)}]^{-1}$ and $t^{(p)}=1$ this is the generalized Newton–Raphson iteration.[27] Methods of this type have received a good deal of attention in the recent literature.[28] The most popular variant, however (Broyden's fs/r quasi Newton method[29]), is unsuitable in the present application because of excessive demands on storage and inefficiency of the procedure for updating $A^{(p)}$. Even with an improved updating procedure[30] the convergence of Eq. 26 was not appreciably accelerated; therefore $A^{(p)}$ was kept constant at an initial approximation $A^{(0)}$ obtained by numerical differencing.

$A^{(p)}$ is a $2l(m-2)$ by $2l(m-2)$ matrix consisting entirely of $(m-2)$ by $(m-2)$ tridiagonal submatrices (some of them null). The method used for the direct solution of Eq. 27 takes advantage of this fact. It is a generalization of the well-known algorithm for reducing tridiagonal systems.[26] At each step in the eliminations $2l$ equations are used simultaneously to eliminate $4l^2$ elements of $A^{(p)}$ (i.e., one subdiagonal element of each submatrix); at each step in the back-substitutions, $2l$ components of $d^{(p)}$ are found simultaneously. This facilitated the rapid evaluation of Eq. 26, with x composed of up to 238 unknowns ($l=7$, $m=19$).

Within the frequency–Mach number domain $fM\leqslant 0.135a/D$ 19 circumferential and radial grid lines

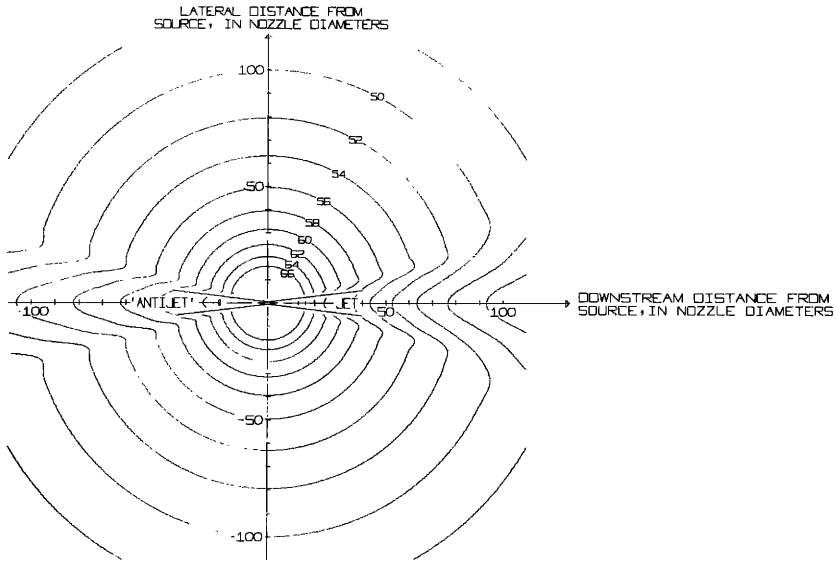

FIG. 2. SPL for $\omega D/\alpha_0 = 1.055$, $M_j = 0.1$. Constant SPL contours at intervals of 2 dB. $(T_{jet} - T_{amb})/T_{amb} = 0$. Distance from nozzle = 0. Program parameters: $M = 19$, $N = 19$, $\tan\theta/\tan\zeta = 0.289$. Frequency: 3000 Hz for $\frac{3}{4}$-in. jet.

($m = n = 19$) sufficed to delineate the solution accurately. The iteration block size required for stability varied from $l = 3$ to $l = 5$ in this regime. For $fM > 0.135a/D$ the discretization error increased rapidly, but any increases in m and n would have led to prohibitive computing time, storage and stability problems. For this regime, therefore, the solution was recomputed for a succession of fan-shaped domains making smaller and smaller angles with the jet axis. Whenever the solution near the axis converged after very few such steps, the result was accepted as accurate. In this way the fM product was pushed up to about $0.28\ a/D$ (less for heated jets).

III. RESULTS AND DISCUSSION

The contour plots of sound-pressure level (SPL) and phase in Figs. 2–4 (interpolated from the finite-difference results) serve to portray the general character of the results. The convergence of the discrete solution with increasing grid density is illustrated in Fig. 5. A

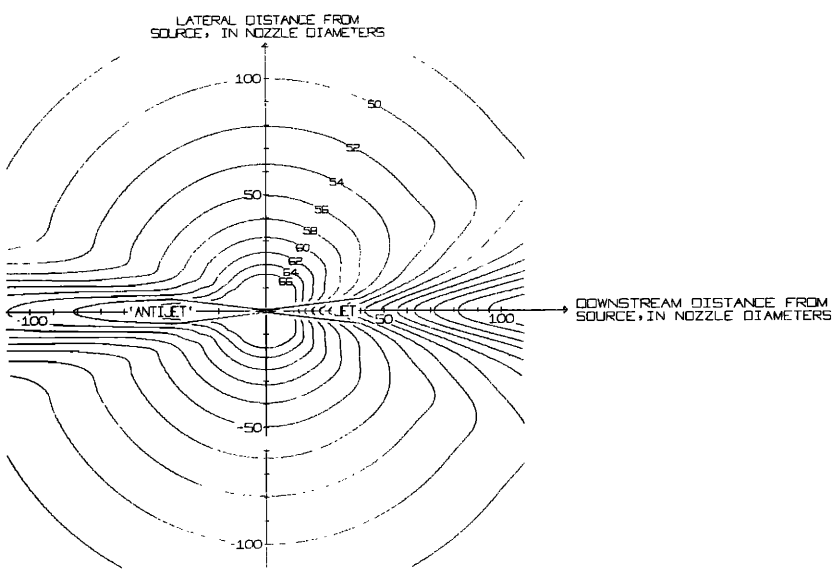

FIG. 3. SPL for $\omega D/\alpha_0 = 1.055$, $M_j = 0.3$. Constant SPL contours at intervals of 2 dB. $(T_{jet} - T_{amb})/T_{amb} = 0$. Distance from nozzle = 0. Program parameters: $M = 19$, $N = 19$, $\tan\theta/\tan\zeta = 0.289$. Frequency: 3000 Hz for $\frac{3}{4}$-in. jet.

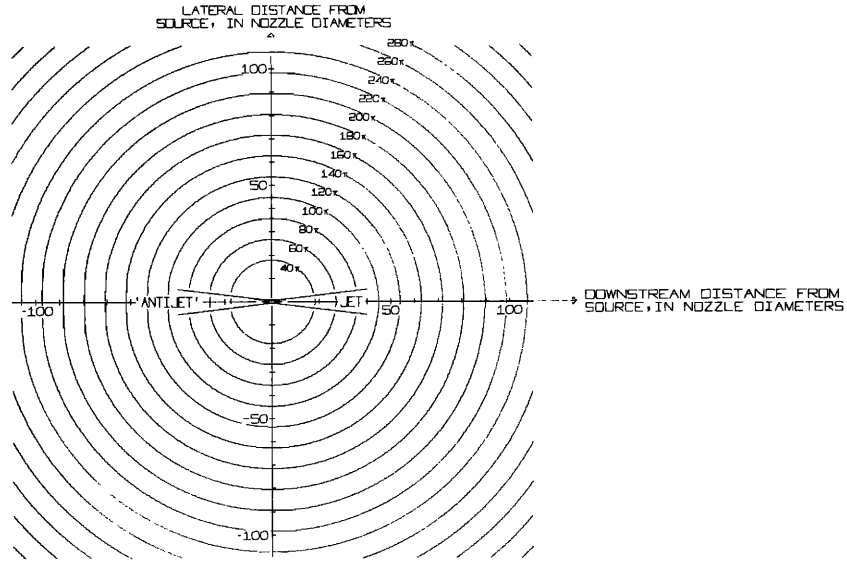

FIG. 4. Phase for $\omega D/\alpha_0 = 7.03$, $M_j = 0.0632$. Constant phase contours at intervals of 20π rad. $(T_{jet} - T_{amb})/T_{amb} = 0$. Distance from nozzle = 0. Program parameters: $M = 19$, $N = 19$, $\tan\theta/\tan\zeta = 0.289$. Frequency: 20 000 Hz for $\frac{3}{4}$-in. jet.

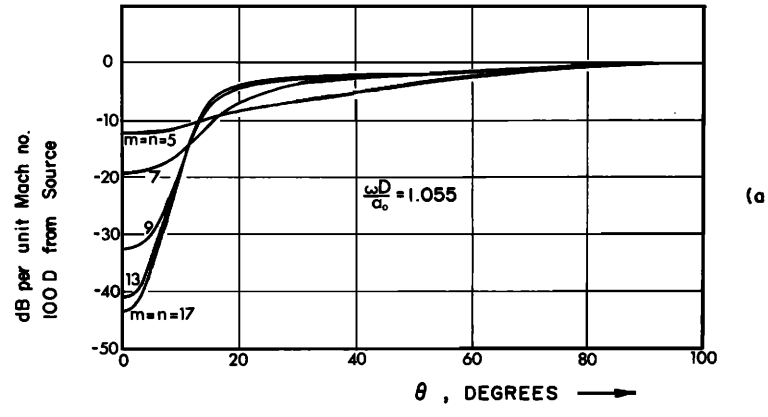

FIG. 5. The behavior of the solution as a function of the number of circumferential and radial grid lines at very low Mach number (a) Behavior of directivity pattern at $100D$. (b) Valley depth at $100D$.

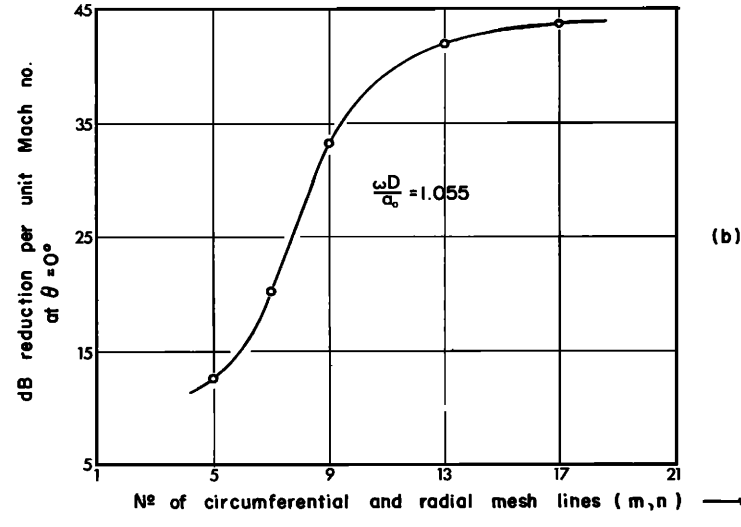

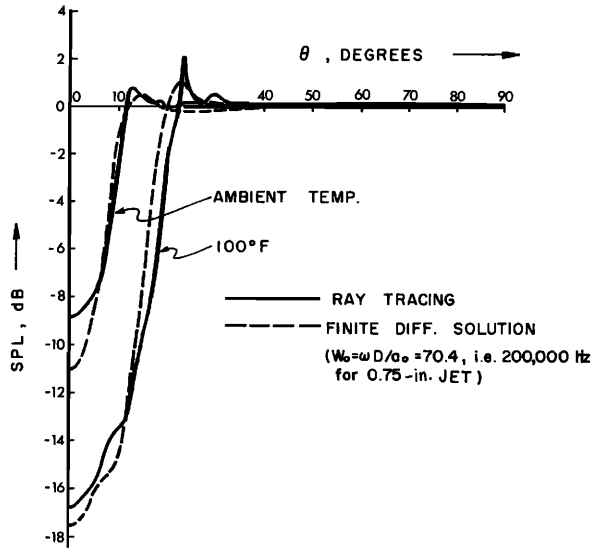

FIG. 6. High-frequency limit of refraction patterns for unheated and slightly heated jet, using ray-tracing (by methods of Ref. 1) and finite difference method. $M_j=0.01$, source at $2D$, observer $100D$ from source.

comparison of finite-difference results and ray-tracing results is shown in Fig. 6 (also phase, Fig. 16). The transition from wave-acoustic behavior was found to be nearly complete at $f\approx 6a/D$ $(D/\lambda\approx 6)$, in the sense that further frequency increases cause only a small fractional change in the decibel depth of the axial valley.

A. Sound-Pressure Level

Figures 7–9 compare computed and measured directivity patterns at $100D$ for several frequencies and Mach numbers.[5] The agreement is good at the lower frequencies and Mach numbers ($fM<\sim 0.065a/D$). When the term $i\omega^{-1}\nabla^2 U\partial\Pi/\partial x_1$ is omitted from Eq. 13, the computed refraction valleys are slightly deeper than those measured; when it is included, the agreement becomes nearly exact for the angular range $-8°\leqslant\theta\leqslant 8°$, but the computed SPL then lies above the measured value for $\theta>8°$. The remaining differences probably stem from the choice of inner boundary conditions. As remarked earlier (Sec. I-B), the nearfield characteristics of the experimental point source are not known with certainty. At the higher frequencies and Mach numbers the computed valley becomes considerably deeper than the measured valley (Fig. 9). Now the behavior of different "simple source" types becomes indistinguishable at sufficiently high frequencies, and the accuracy of the wave equation is known to improve with increasing frequency; therefore, these discrepancies are attributed to

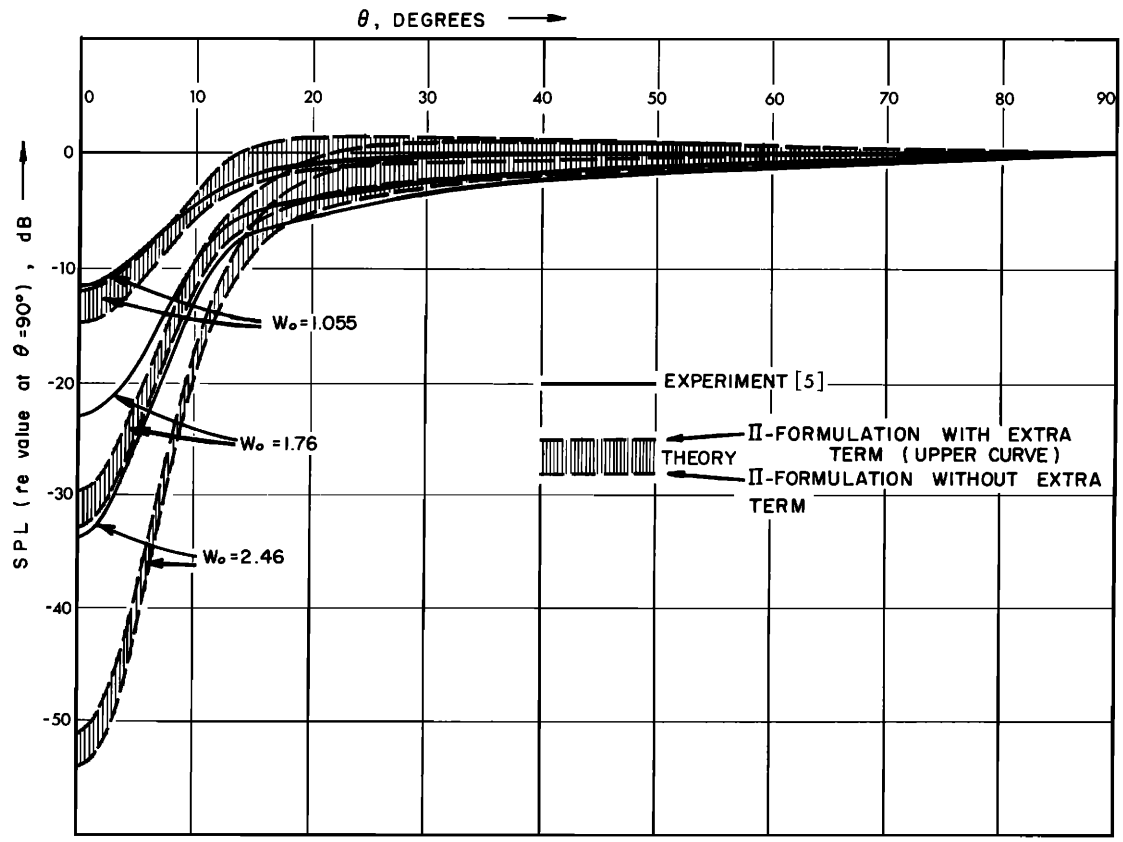

FIG. 7. Comparison of computed and experimental refraction patterns for several frequencies ($W_0=\omega D/a_0=1.055$, 1.76, 2.46, i.e. 3000 Hz, 5000 Hz, 7000 Hz for 0.75-in. jet). $M_j=0.3$, temperature ambient, source at $2D$, observer $100D$ from source.

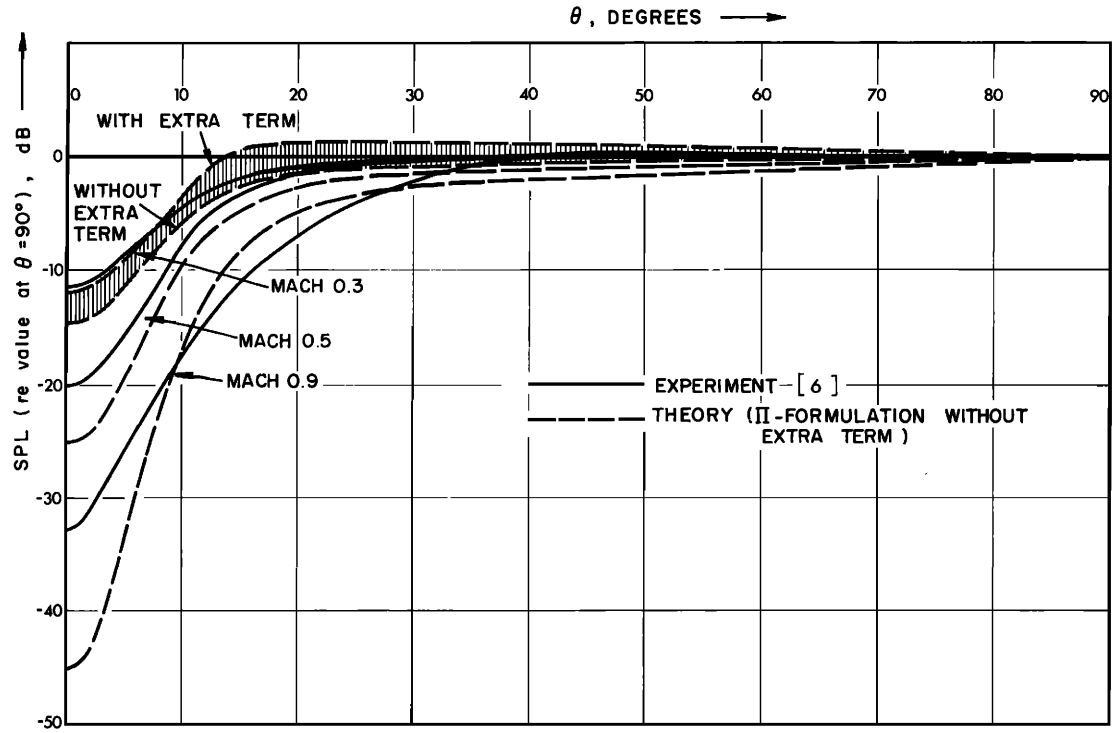

FIG. 8. Comparison of computed and experimental refraction patterns for several Mach numbers (M_j=0.3, 0.5, 0.9). $W_0=\omega D/a_0$ =1.055 (3000 Hz for 0.75-in. jet), temperature ambient, source at $2D$, observer $100D$ from source.

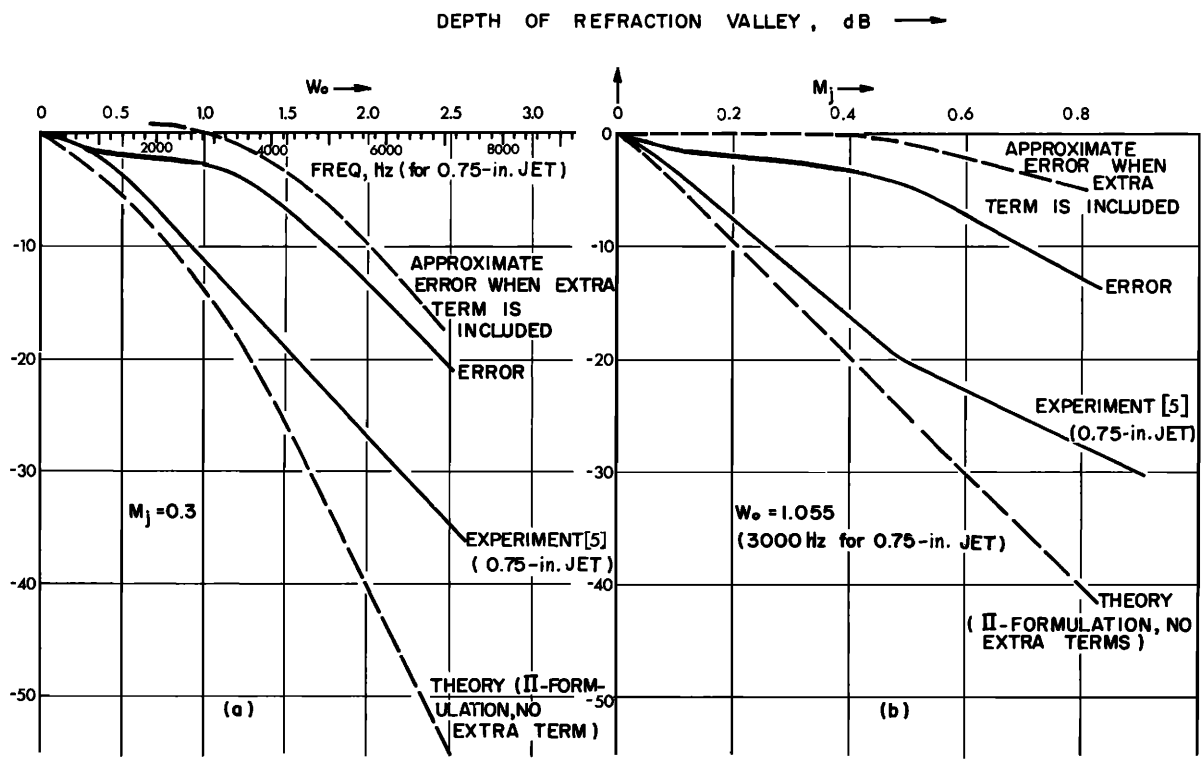

FIG. 9. Depth of refraction valley as a function of (a) frequency ($W_0=\omega D/a_0$) and (b) Mach number. The extra term referred to is $i\omega^{-1}\nabla^2 U\partial\Pi/\partial x_1$. Source at $2D$, SPL measured $100D$ from source. Note that when the valley becomes deeper than about 20 dB, the error grows rapidly.

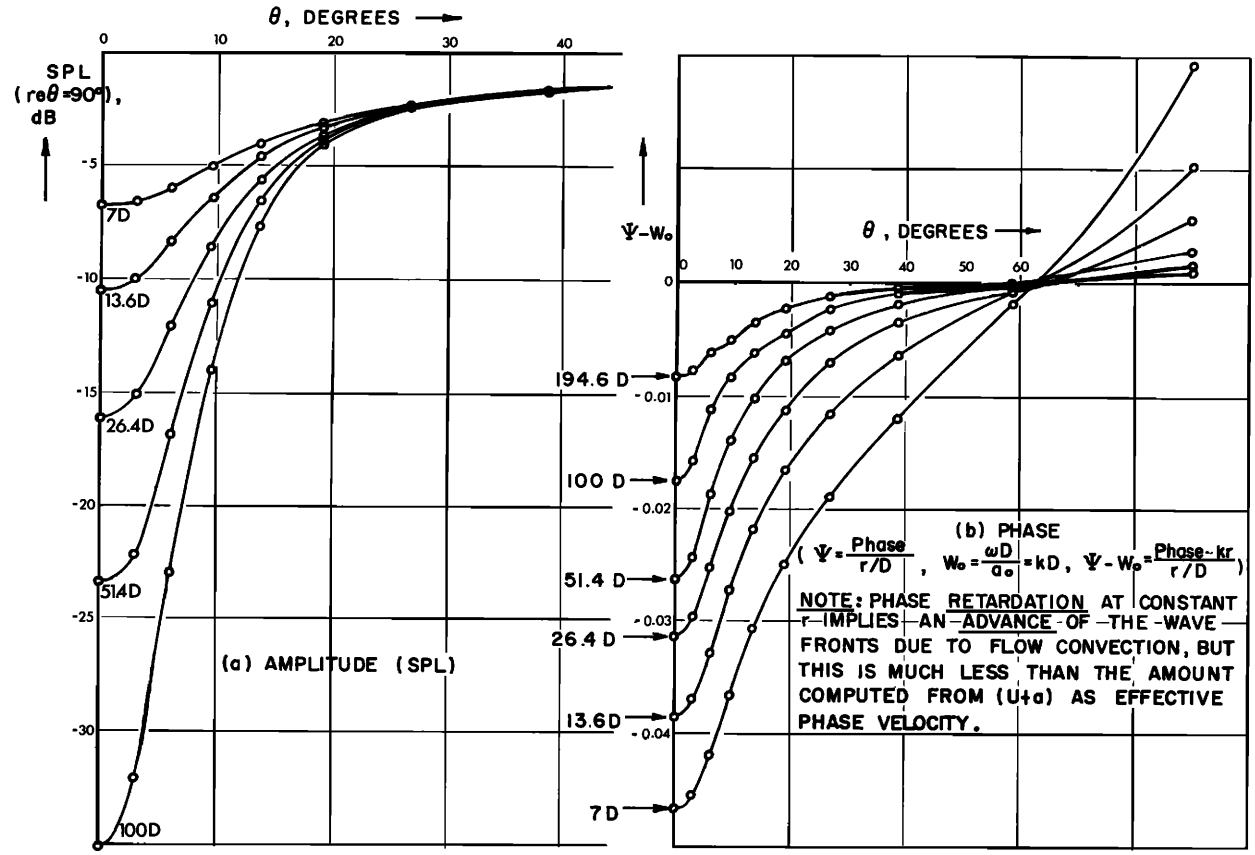

FIG. 10. Circumferential variation of amplitude and phase at several distances; fixed parameters: $W_0=1.055$ (3000 Hz for $\frac{3}{4}$-in. jet), $M_j=0.7$, source at $2D$, temperature ambient.

experimental error. In particular, it is postulated that the measured directivity is a superposition of the true refracted field and a weak secondary field caused by reflections from experimental equipment. This secondary field has only a shallow axial valley because of the wide distribution of reflecting surfaces. When the true valley depth becomes deeper than the secondary field (this appears to occur at a valley depth of about 20 dB), the apparent valley depth is constrained to the level of the secondary field.

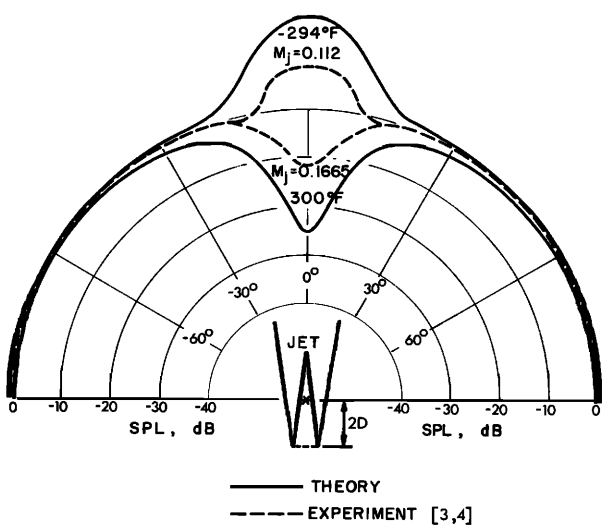

FIG. 11. Polar plots of theoretical and experimental refraction patterns for hot and cooled jets. $W_0=\omega D/a_0=1.055$ (3000 Hz for 0.75-in. jet), observer $100D$ from source.

Except at the very highest (near ray-acoustic) frequencies the width of the axial valley is virtually frequency-independent, reaching half its decibel depth, relative to the value at $\theta=30°$, at $\theta=7.7°$. The width changes little with distance from the source, at least for $r\geqslant 7D$ [Fig. 10(a)].

The depth of the valley, however, continues to grow for very large distances from the source. For example, at $f=0.17a/D$ the decibel depth doubles beyond $100D$. Beyond $5000D$, little further change occurs.

The numerical results for heated and cooled jets (Figs. 11–13) show more powerful refraction effects than were experimentally observed. As the finite-difference results for heated jets are supported by ray-tracing results at the high-frequency limit, the differences are tentatively attributed to the effects of buoyancy on real heated or cooled jets. The buoyant forces spoil the sym-

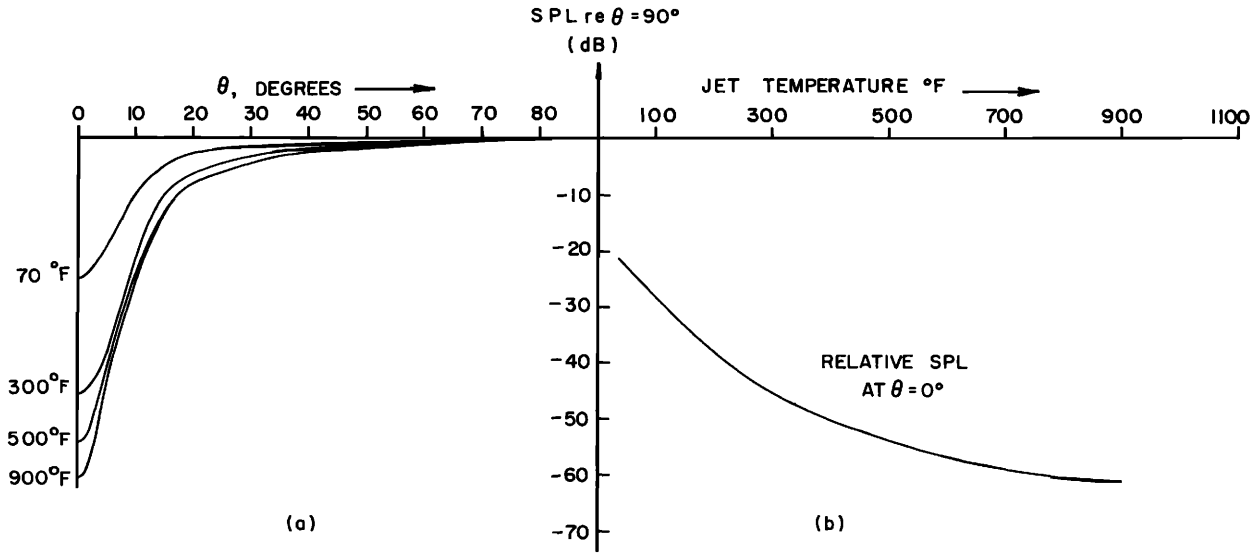

FIG. 12. Computed temperature effect ($\omega D/a_0=1.055$, $M_j=0.5$, source at $2D$). (a) Downstream directivity at $100D$. (b) Variation of SPL at $\theta=0°$, $r=100D$ with temperature.

metry of a horizontal jet by curving the center line and may thus reduce refraction.

Figure 14 shows the variation of valley depth with source position at several frequencies. Experiments[3] had revealed the surprising fact that refraction varies little for a range of axial source positions of interest for jet noise (0–8D). According to computed results there is actually an initial increase in refraction as the source is moved downstream. This may indicate that reflections in the initial part of the jet, which tend to cause axial enhancement of the intensity, more than offset refraction effects there.

The following simple procedure may be used to estimate SPL's in approximate agreement with computed results (for $f\leqslant 0.55\ a/D$).

(1) Find S_1 as the ordinate corresponding to the given $W_0(=\omega D/a_0)$ for the lower broken line in Fig. 9(a). Use the linear continuation of the curve if necessary.

(2) $S_2=M_jS_1/0.3$.

(3) $S_3=S_2+M_j\times$(ordinate corresponding to the appropriate distance in Fig. 15).[31]

(4) Find the ordinate S_4 corresponding to θ on the $100D$ curve in Fig. 10(a).

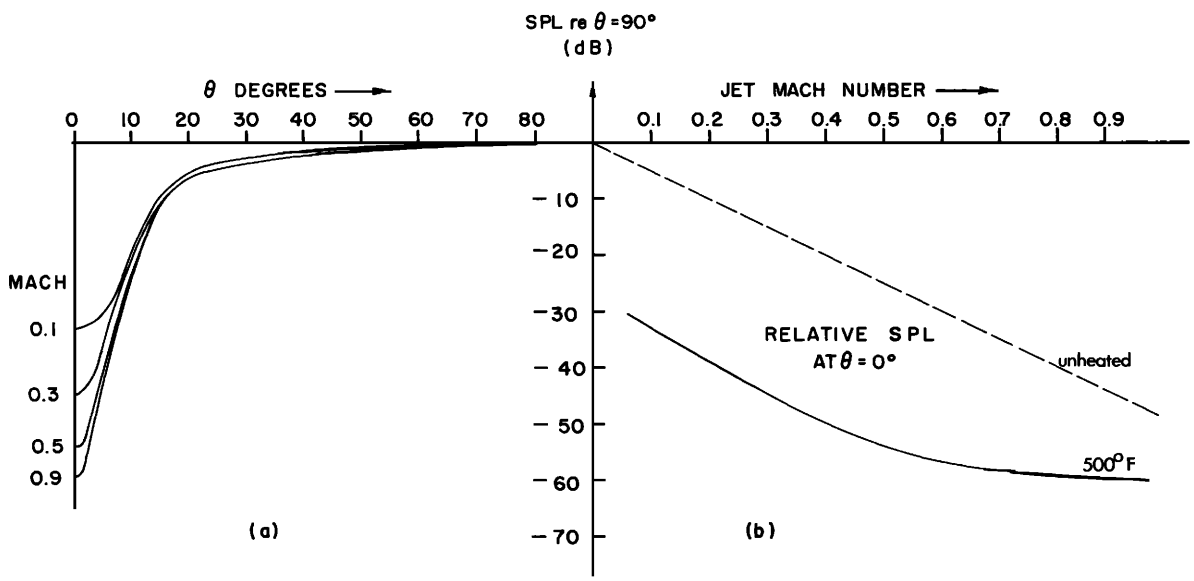

FIG. 13. Directivity patterns for a hot jet at various Mach numbers. Fixed parameters: $\omega D/a_0=1.055$, jet temperature=500°F, source at $2D$. (a) Downstream directivity at $100D$. (b) Variation of SPL at $\theta=0°$, $r=100D$ with Mach number.

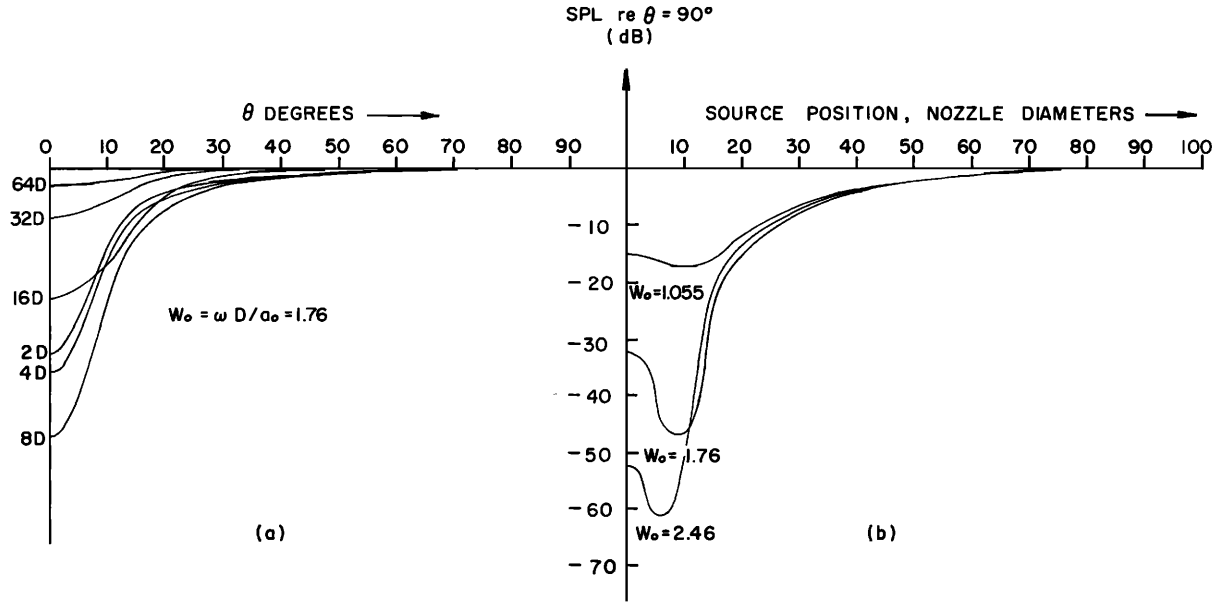

FIG. 14. Effect of source position on refraction valley. Fixed parameters: $M_j=0.3$, temperature ambient. (a) Directivities for a succession of axial source positions with source–observer distance fixed at $100D$. (b) SPL at $\theta=0°$, $100D$ from the nozzle, as a function of source position (for three frequencies).

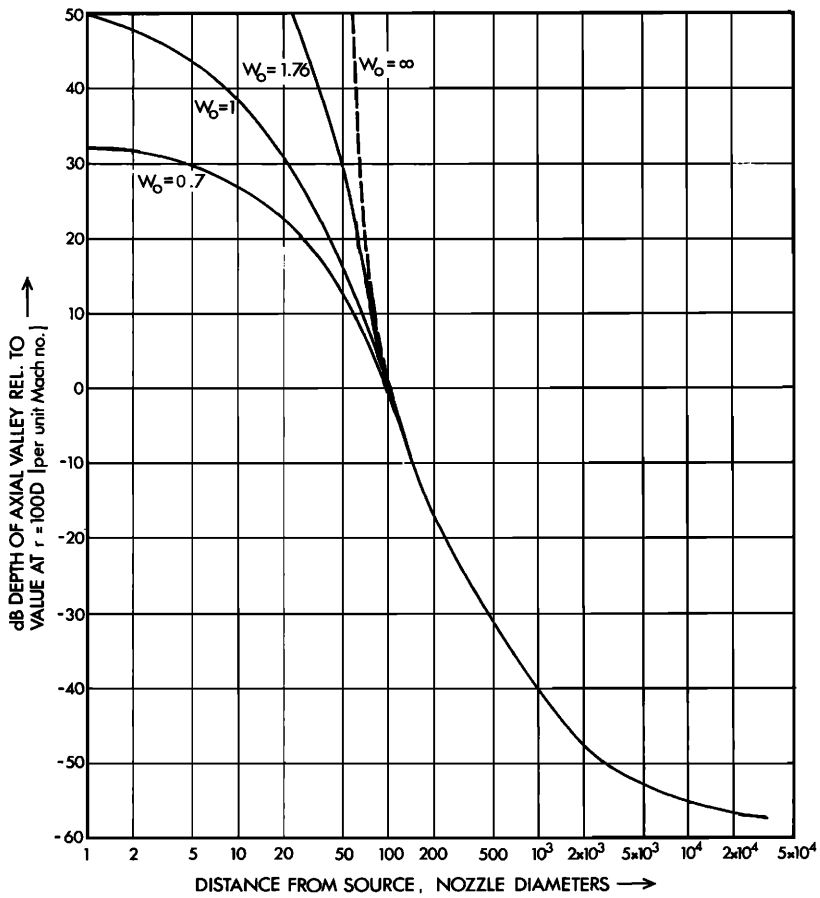

FIG. 15. Deepening of axial valley with distance, per unit Mach No. (approximate, based on several frequencies). Temperature ambient, $W_0=\omega D/a_0$.

(5) $S_5=S_3S_4/35.1$.

(6) SPL relative to $\theta=90°\approx S_5+10M_j\cos\theta$ (correction for the last term in Eq. 13).

This estimate applies to unheated jets. Heated jets pose a problem, because of the discrepancies with experiment and also because the SPL is apparently not linear in Mach number for hot jets [Fig. 13(b)]. As a crude correction one may add

$$[1.8-M_j-(0.692-1.6M_j+M_j^2)^{\frac{1}{2}}]\times\left(\frac{19.5}{T_j/T_0-0.565}-45\right)\text{dB}$$

to the depth of the valley and scale up values at $\theta\neq 0$ proportionately. It should be kept in mind, however, that this decibel correction may be too large by a factor of 2 or more for a real jet.

B. Phase

It was shown in Ref. 1 that the surfaces of constant phase must become more and more nearly spherical far from the source, even though the phase differential between $\theta=0$ and $\theta=\pi/2$ increases without limit. It turns out that the distortion of these surfaces from spherical shape is slight at all distances from the source, except for the very highest frequencies. For example, at $f=0.17a/D$ the axial phase lag at $100D$ relative to quiescent values is only 1.42 rad, as compared to a lag of 10.6 rad that would be observed if the axial phase velocity were the sum of flow speed and sound speed. The reason is that the bulk of the sound near the axis has leaked in by diffraction from outside, so that it tends to be phase-locked to the outside pattern. The circumferential phase variation at several distances is shown in Fig. 10(b). The axial phase variation for a large range of frequencies is plotted in Fig. 16. No procedure for reconstructing computed values, like that given for the SPL, has been devised for the phase. This was considered unnecessary since for jet noise applications the phase information can usually be dispensed with, as will be seen below.

C. Application to Jet Noise

In Ref. 6 it was assumed that the directivity pattern for jet noise at a particular frequency (i.e., the variation of SPL with θ, in decibels) is essentially the directivity pattern without allowance for refraction plus the corresponding directivity pattern for a simple source on the jet axis.

Actually, the correct expression for the farfield jet noise intensity at **x**, due to unit volume at **y**, at fre-

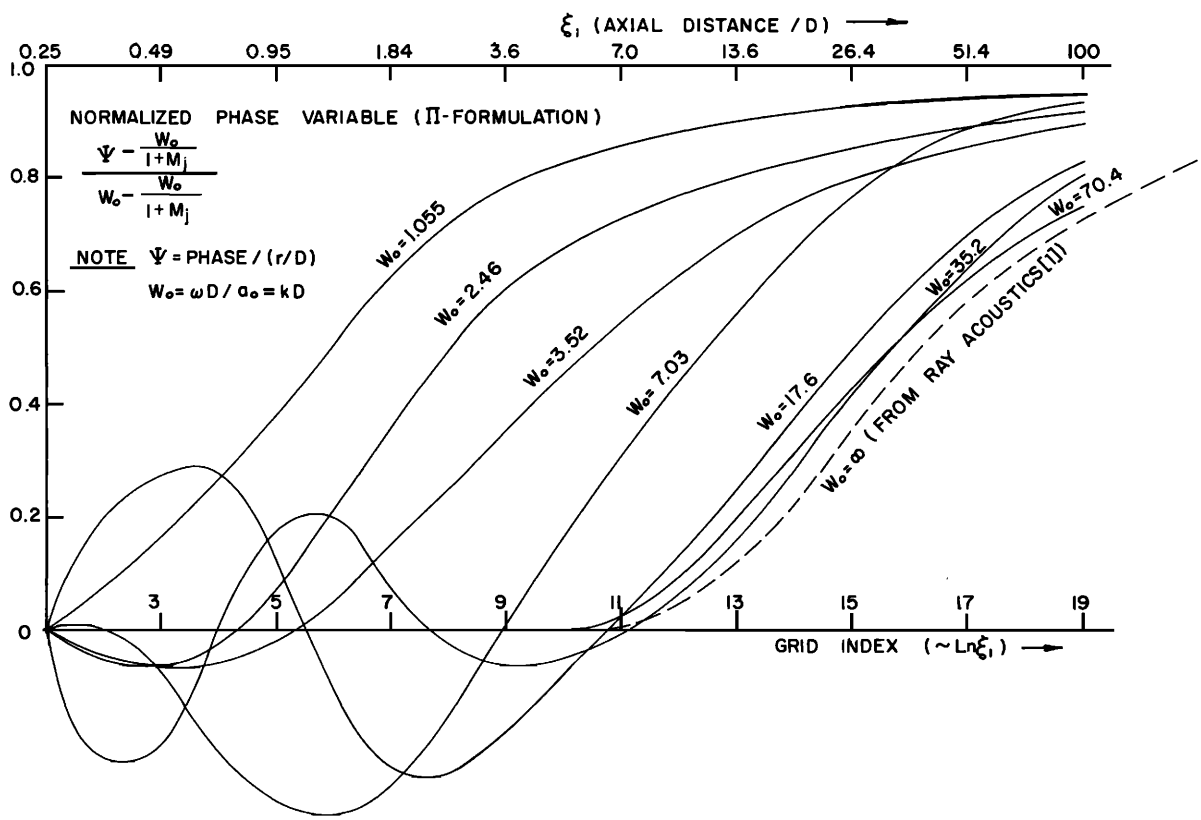

FIG. 16. Variation of phase variable (normalized) along jet axis. The Mach No. is not identical for all examples shown, though always <0.1. Variations of the curves are slight in this range.

quency f, is[22]

$$I(\mathbf{x},\mathbf{y},f)=\frac{G(\mathbf{x},\mathbf{y},f)}{16\pi^2x^2\rho_0a_0}\int_{-\infty}^{\infty}d\tau\int_{-\infty}^{\infty}d^3\mathbf{y}'G^*(\mathbf{x},\mathbf{y},f)$$
$$\times\langle P(\mathbf{y},t)P(\mathbf{y}',t+\tau)\rangle_{\mathrm{av}}$$
$$\times\exp\{-2\pi if[\tau+(|\mathbf{x}-\mathbf{y}'|-|\mathbf{x}-\mathbf{y}|)/a_0]\},\quad(28)$$

where[8,10] $P(\mathbf{y},t)=-(\bar{a}^2)^{-1}\bar{D}^2p^{(0)}/\bar{D}t^2$ ($\bar{D}/\bar{D}t$ denotes the time derivative following the mean flow and the angular brackets denote averaging over t) and $|\mathbf{x}-\mathbf{y}|^{-1}G(\mathbf{x},\mathbf{y},f)\times\exp(-2\pi ift)$ ($=g'$, say) is a discrete-tone Green's function for the pressure formulation of the convected wave equation. That is, it corresponds to a source term of type $\delta(\mathbf{x}-\mathbf{y})\exp(-2\pi ift)$ added on to the right of Eq. 12.

The pressure patterns

$$|\mathbf{x}-\mathbf{y}|^{-1}\chi\exp[i\Phi-2\pi if(t+|\mathbf{x}-\mathbf{y}|/a_0)]$$

($=g$, say) calculated herein, however, correspond to a discrete-tone Green's function for the acoustic *potential*, or equivalently, to a source term of type

$$D[\delta(\mathbf{x}-\mathbf{y})\exp(-2\pi ift)]/Dt$$

in the pressure formulation Eq. 12;[32] this is implicit in the use of Eq. 21 as inner boundary condition. The relationship between g and g' is easily shown to be $g=-2\pi ifg'-U\partial g'/\partial y_1$; this has the approximate solution $g'\approx(i/2\pi f)(1-M\cos\theta)^{-1}g$ in the farfield, assuming that the main effect on g of a source displacement Δy_1 is a phase shift $-(2\pi f/a_0)\Delta y_1\cos\theta$ (i.e., the jet-off value). This assumption is restated as (2) below.

Now the assumption that a refraction correction can be added on as in Ref. 6 turns out to be equivalent to taking G^* *outside* the integral in Eq. 28. This can be justified if (1) sources at points $\mathbf{y}$ and $\mathbf{y}'$ generate approximately the same SPL at a distant field point $\mathbf{x}$, where $\mathbf{y}$ and $\mathbf{y}'$ lie within the main region of sound generation; and (2) variations in the cumulative phase difference Φ between $\mathbf{x}$ and $\mathbf{y}$ are small in the sense

$$|\Phi(\mathbf{x},\mathbf{y},f)-\Phi(\mathbf{x},\mathbf{y}',f)-2\pi f(|\mathbf{x}-\mathbf{y}|-|\mathbf{x}-\mathbf{y}'|)/a_0|\ll\pi$$

for $\mathbf{y}$, $\mathbf{y}'$ within the volume swept out by an eddy during its lifetime.

Detailed examination of computed amplitude and phase data suggests that for $f\leqslant0.4a/D$ criteria (1) and (2) should be roughly satisfied.[33] At moderate frequencies, therefore, it should be possible to use

$$20\log_{10}|G(\mathbf{x},\mathbf{y},f)|\sim20\log_{10}[\chi/(1-M\cos\theta)]\ \mathrm{dB},$$

where M is the Mach number at the source point, as a refraction correction to be added onto the "basic" directivity[9,10,34] modified by convection effects.[20,8,10,35] In principle this provides a purely theoretical procedure for computing jet noise directivity patterns. Note the downstream "bulge" contributed by the term $(1-M\cos\theta)^{-1}$ above; this augments a similar (but shallower) bulge associated with the "extra terms" in Eqs. 12 and 13, and diminishes the refraction valley depth at the higher Mach numbers. Since experimental point source refraction patterns lack this downstream bulge, "naïve" refraction corrections to jet noise patterns on the basis of these data are presumably too large at high Mach numbers. A recent amendment[36] of the experimental refraction corrections, designed to remedy infractions of energy conservation, appears to confirm this view.

In summary, a convected wave equation appropriate to the propagation of sound in a jet flow has been derived. Solutions by finite-difference methods were obtained for $fM\leqslant0.28a/D$. The results support and extend experimental results showing that the axial valley in jet noise is due to refraction.

ACKNOWLEDGMENTS

The work reported was suggested and supervised by Professor H. S. Ribner. His invaluable help in its development and interpretation is gratefully acknowledged. The research was sponsored by the National Research Council of Canada under NRC grant No. A2003, and by the Air Force Office of Scientific Research, Office of Aerospace Research, United States Air Force, under AFOSR grant No. AF-AFOSR 67-0672A.

* Present address: Dept. of Computing Science, University of Alberta, Edmonton 7, Alta., Canada.

[1] L. K. Schubert, "Numerical Study of Sound Refraction by a Jet Flow I. Ray Acoustics," J. Acoust. Soc. Amer. **51**, 439–446 (1972).

[2] J. Atvars, L. K. Schubert, and H. S. Ribner, "Refraction of Sound from a Point Source Placed in an Air Jet," J. Acoust. Soc. Amer. **37**, 168–170 (1965).

[3] J. Atvars, L. K. Schubert, and H. S. Ribner, "Refraction of Sound from a Point Source Placed in an Air Jet," AIAA Paper No. 65-82, AIAA Aerospace Sci. Meeting, 2nd New York, 25–27 Jan. 1965.

[4] E. Grande, "Refraction of Injected Sound by a Very Cold Nitrogen Jet," J. Acoust. Soc. Amer. **38**, 1063–1064 (1965).

[5] J. Atvars, L. K. Schubert, E. Grande, and H. S. Ribner, "Refraction of Sound by Jet Flow and Jet Temperature," NASA CR-494 (May 1966).

[6] E. Grande, "Refraction of Sound by Jet Flow and Jet Temperature II," Univ. Toronto Inst. Aerospace Studies, Tech. Note 110 (1966); also NASA CR-840 (Aug. 1967).

[7] A. Powell, "Survey of Experiments on Jet Noise," Aircraft Eng. **26**, 2–9 (1954).

[8] H. S. Ribner, "Aerodynamic Sound from Fluid Dilatations—A Theory of the Sound from Jets and Other Flows," Univ. Toronto Inst. Aerospace Studies, Rep. 86 (AFOSR TN 3430) (1965).

[9] H. S. Ribner, "On Spectra and Directivity of Jet Noise," J. Acoust. Soc. Amer. **35**, 614–616 (1963).

[10] H. S. Ribner, "The Generation of Sound by Turbulent Jets," Advan. Appl. Mech. **8**, 103–182 (1964).

[11] The source-jet configuration is illustrated in Ref. 1; the velocity and temperature profiles also are specified there.

[12] H. S. Ribner, "Reflection, Transmission and Amplification of Sound by a Moving Medium," J. Acoust. Soc. Amer. **29**, 435–441 (1957).

[13] P. Gottlieb, "Acoustics in Moving Media," PhD thesis, Physics Dept., Mass. Inst. of Tech. (1959); also "Sound Source Near a Velocity Discontinuity," J. Acoust. Soc. Amer. **32**, 1117–1122 (1960).

[14] G. Moretti and S. Slutsky, "The Noise Field of a Subsonic Jet," Gen. Appl. Sci. Lab., GASL Tech. Rep. 150 (AFOSR TN-59-1310) (1959).

[15] S. Slutsky and J. Tamagno, "Sound Field Distribution About a Jet," Gen. Appl. Sci. Lab., Tech. Rep. 259 (AFOSR TN 1935) (1961).

[16] S. Slutsky, "Acoustic Field of a Cylindrical Jet due to a Distribution of Random Sources or Quadrupoles," Gen. Appl. Sci. Lab., Tech. Rep. 281 (1962).

[17] D. I. Blokhintsev, "Acoustics of a Nonhomogeneous Moving Medium," in Russian (1946), translated by Natl. Adv. Comm. Aeron. as NACA T.M. 1399 (1956).

[18] D. C. Pridmore-Brown and U. Ingard, "Tentative Method for Calculation of the Sound Field about a Source over Ground Considering Diffraction and Scattering into Shadow Zones," NACA TN 3779 (1956).

[19] $-\Delta p/p_0 \approx \rho_0 \overline{v_z^2}$. The maximum of $\overline{v_z^2}/U_j^2$ is 0.0056 at $x_1 = 20D$ [see A. A. Townsend, *The Structure of Turbulent Shear Flow* (Cambridge U. P., Cambridge, England, 1956)]. This corresponds to a fractional pressure change $0.0056\,\gamma(U_j/a_0)^2$ on the axis.

[20] M. J. Lighthill, "On Sound Generated Aerodynamically, I—General Theory," Proc. Roy. Soc. (London) Ser. A **211**, 564–578 (1952); "II—Turbulence as a Source of Sound," Proc. Roy. Soc. (London) Ser. A **222**, 1–32 (1954).

[21] O. M. Phillips, "On the Generation of Sound by Supersonic Turbulent Shear Layers," J. Fluid Mech. **9**, 1–28 (1960).

[22] L. K. Schubert, "Refraction of Sound by a Jet: a Numerical Study," Univ. Toronto Inst. Aerospace Stud., Tech. Note 144 (1969).

[23] In most cases $\alpha = 0.538$ was near-optimal.

[24] E. W. Graham and B. B. Graham, "A Note on Theoretical Acoustical Sources in Motion," J. Fluid Mech. **49**, 481–488 (1971).

[25] Some solutions were extended to $\sigma = 20\,000$ by using computed values at $51.4D$ as inner boundary values on an expanded grid. The writer is indebted to C. S. Matthias for suggesting this method.

[26] R. S. Varga, *Matrix Iterative Analysis* (Prentice–Hall, Englewood Cliffs, N. J., 1962).

[27] P. Wolfe, "The Secant Method for Simultaneous Nonlinear Equations," Comm. Assoc. Comp. Mach. **2**, 12–13 (1959).

[28] E. M. Rosen, "A Review of Quasi-Newton Methods for Nonlinear Equation Solving and Unconstrained Optimization," *Proceedings of the 21st National Conference of the ACM* (Thompson Book Co., Washington, D. C., 1966), pp. 37–41.

[29] C. G. Broyden, "A Class of Methods for Solving Nonlinear Simultaneous Equations," Math. Comp. **19**, 577–593 (1965).

[30] L. K. Schubert, "Modification of a Quasi-Newton Method for Nonlinear Equations with a Sparse Jacobian," Math. Comp. **24**, 27–30 (1970).

[31] This corrects step 3 in Ref. 22.

[32] This point was missed in Ref. 22.

[33] The computed results are for sources on the jet axis. The fact that the major part of the noise radiated by a jet actually originates at points displaced from the axis probably does not affect the frequency bound $f \leqslant 0.4a/D$ adversely. In the first place, experiments indicate that the average intensity due to symmetrically disposed sources off the axis is nearly the same as the intensity for a centered source (Ref. 3). Secondly, the maximum phase shift induced by the flow is likely to be diminished, rather than increased, by lateral source displacements (because the axial symmetry is spoiled).

[34] H. S. Ribner, "Quadrupole Correlations Governing the Pattern of Jet Noise," J. Fluid Mech. **38**, 1–24 (1969).

[35] J. E. F. Williams, "The Noise from Turbulence Convected at High Speed," Phil. Trans. Roy. Soc. London, Ser. A **255**, 469–503 (1963).

[36] Section E-4, UTIAS Ann. Prog. Rep., Univ. Toronto, Inst. Aerospace Studies, (1970).